Thermal dynamics assessment of vanadium redox flow batteries and thermal management by active temperature control

Hao Wang<sup>a,\*</sup>, Wen L. Soong<sup>a</sup>, S. Ali Pourmousavi<sup>a</sup>, Xinan Zhang<sup>b</sup>, Nesimi Ertugrul<sup>a</sup>, Bingyu Xiong<sup>c</sup>

<sup>a</sup>School of Electrical & Electronic Engineering, The University of Adelaide, Australia  $^b$ School of Engineering, The University of Western Australia, Australia

<sup>c</sup>School of Automation, Wuhan University of Technology, China

**Abstract** 

Understanding the thermal dynamics of vanadium redox flow batteries (VRFB) is critical in pre-

venting the thermal precipitation of vanadium species that result in capacity fading and unsafe

operation. This paper presents a comprehensive thermal model of a 5kW/60kWh VRFB system

by considering the impact of current, ambient temperature and electrolyte flow rate to investigate

the dynamic and steady-state thermal conditions of VRFB systems. To analyse the feasibility of

using air conditioners for effective thermal management, a room temperature model is proposed

to simulate the room temperature variations with air flow cooling. Finally, based on the proposed

VRFB thermal model and the room temperature model, two case studies with different tempera-

ture profiles are presented to evaluate the performance of the proposed model. Most importantly,

an improved cooling strategy is proposed and validated for the two case studies considering the

different thermal behaviours of VRFBs during charging and discharging. The simulation results

show that the proposed strategy can save up to 48% on air conditioner consumption. Also, the

modelling work presented in this paper is useful for studying the thermal dynamics of a VRFB

system after many operational cycles and providing guidance for the thermal management of

VRFBs in real-world applications.

Keywords: Vanadium redox flow battery, battery thermal modelling, thermal management,

battery thermal dynamics, air flow cooling.

\*Corresponding Author

Email address: hao.wang05@adelaide.edu.au

Preprint submitted to Elsevier

March 30, 2023

Nomenclature		k	Diffusion coefficient (m <sup>2</sup> s <sup>-1</sup> )	
		$k_m$	Mass transfer coefficient (m $s^{-1}$ )	
$\Delta G^\Theta$	Gibbs free reaction enthalpy (J)	L	Length (m)	
$\Delta H_r^{\Theta}$	Molar reaction enthalpy (J)	$M_{air}$	Total air mass inside the room (kg)	
$\Delta S_r^{\Theta}$	Molar reaction entropy (J K <sup>-1</sup> )	$M_{dot}$	Air mass flow through air conditioner	
$\Delta S_r$			$(kg s^{-1})$	
$\eta_a$	Activation overpotential (V)	N	Number of cells	
$\eta_{con}$	Concentration overpotential (V)	Q	Electrolyte flow rate (L s <sup>-1</sup> )	
ho	Electrolyte density (kg m <sup>-3</sup> )	Q	Thermal energy (J)	
A	Surface area (m <sup>2</sup> )	R	Gas constant (J $mol^{-1} K^{-1}$ )	
C	Heat capacity of air (J kg <sup>-1</sup> K <sup>-1</sup> )	r	Cell ohmic resistivity ( $\Omega$ m $^2$ )	
c	Concentration (mol L <sup>-1</sup> )	$r^{'}$	Overall cell resistivity ( $\Omega$ m <sup>2</sup> )	
$C_p$	Specific heat capacity of electrolyte	$R_s$	Overall stack resistance $(\Omega)$	
•	$(J kg^{-1}K^{-1})$	S	Active area (m <sup>2</sup> )	
D	Thickness of membrane (m)	SOC	State of charge	
E	Electric potential (V)	T	Temperature (K)	
$E^{0'}$	Formal potential (V)	t	Time (s)	
$E^0$	Standard cell potential (V)	V	Volume (L)	
	•	W	Width (m)	
EER	Energy efficiency ratio	z	Number of electrons involved in the redox	
F	Faraday's constant (C mol <sup>-1</sup> )		reactions	
Н	Height (m)	Subscr	Subscripts	
h	Heat transfer coefficient of concrete	(1)	Self discharge reaction 1	
	$(W m^{-2} K^{-1})$	(2)	Self discharge reaction 2	
I	Current (A)	(3)	Self discharge reaction 3	
i	Current density (A m <sup>-2</sup> )	(4)	Self discharge reaction 4	
	•	2		

a	Activation overpotentials	4	$VO^{2+}$	
ac	Air conditioner	5	$VO_2^+$	
con	Concentration overpotentials	Superso	uperscripts	
e	Electrode	Θ	Standard	
N	Negative side	OCV	Open circuit voltage	
out	Outside	S	Stack	
P	Positive side	t	Tank	
r	Reaction			
2	V <sup>2+</sup>	+	Positive half-cell	
3	$V^{3+}$	-	Negative half-cell	

#### 1. Introduction

With the increasing demand for renewable energy (RE), large-scale energy storage systems (ESSs) are essential to enable a higher uptake of RE and efficiently utilise these resources towards a sustainable energy system. Among the different mainstream ESSs, vanadium redox flow battery (VRFB) is one of the most reliable technologies among the flow battery family. The VRFB has several technical advantages, including low cost, simple design, long life span, independent capacity and rated power design, no cross-contamination issues and ready electrolyte recycling, which makes it a promising solution for large-scale storage applications. The thermal management for contemporary battery technologies is important to ensure their high performance and reliability over a long operational period. The thermal modelling of a VRFB system is critical to conduct effective thermal management to stabilise the electrolyte performance, prevent thermal precipitation of active species and maintain the overall efficiency of this VRFB system.

Previous studies on the thermal stability of the VRFB electrolyte have been conducted to show the significance of developing thermal models for efficient thermal management. In [1], a study on the cell electrolyte has shown that the thermal precipitation of  $V_5^+$  can happen when the temperature exceeds  $40^{\circ}$  C, while the precipitation of  $V_2^+$  and  $V_3^+$  can occur if the temperature 3 is lower than 5°C. The precipitation of vanadium species is an irreversible process that risks the reliability of the VRFB system by causing membrane damage, stack channel congestion and capacity fading [2]. Although several inhibitors have been developed for the electrolytes to reduce the thermal precipitation, as reported in [3, 4]. However, these studies are carried out in an ideal experimental environment by formulating electrolyte solutions with different molarity of vanadium species in a thermostat but neglecting the variations of electrolyte temperature and active species during the continuous operation in real applications. Moreover, the difference in electrolyte solution design and precipitation measurement method can cause different results in reporting the thermal stability tolerance of electrolytes in [1, 5]. As a result, most thermal model studies agreed that 40°C is the safe limit to prevent thermal precipitation, as reported in [1, 2, 6, 7, 8, 9].

In recent years, several papers established the thermal modelling of VRFB systems. In [8], a primary thermal model considering the configurations of a VRFB system is presented to simulate its thermal dynamics. Tang et al. improved this thermal model and carried out several case studies to illustrate the effect of membrane design and flow rate on thermal dynamics. However, these two thermal models do not take the reversible entropic heat from the main chemical reactions into account. In [9], Wei et al. proposed a dynamic thermal-hydraulic model to study the thermal-hydraulic model with different stack flow pattern designs. Recently, Bhattacharjee et al. and Khaki et al. presented two simple thermal models in [6] and [10] correspondingly based on the primary model in [8]. These two simple thermal models are validated via experimental data and show promising results in estimating the thermal dynamics of VRFBs. Trovo et al. [7] established a complete thermal model for an industrial-scale VRFB system to simulate the operation in high-current applications. Here, an important conclusion in such cases is that it is necessary to have active cooling to prevent thermal precipitation, where the high-current discharging process is the main reason causing the electrolyte temperature rise.

Although the necessity of utilising active cooling for efficient thermal management has been drawn in the above-mentioned papers, only a few papers introduced the design of active cooling strategies and heat exchangers for VRFBs. For instance, Wei et al. designed a shell and tube

heat exchanger for active electrolyte cooling in [11]. A foster network is developed here to model the thermal behaviour during the cooling action, and cooling performance by air flow and water is shown to reduce the electrolyte temperature by up to 7°C. It is worth mentioning that air flow cooling and liquid cooling have been commonly used for lithium-ion and other solid-state batteries in electric vehicles (EV) and other advanced applications, as reported in [12, 13]. Nevertheless, for most of the modern commercial VRFB systems, there are no integrated cooling devices, and the most commonly-used cooling method is air flow cooling by using air conditioners [14]. Using air conditioners to manage the electrolyte temperature of the VRFB system has been considered in on-site applications. The effectiveness of using air conditioners for electrolyte cooling is worth investigating, and improved cooling strategies are needed to reduce the power consumption of air conditioners.

To investigate the thermal dynamics of VRFB systems and the effectiveness of using an air conditioner for thermal management, a comprehensive multi-physics VRFB thermal model is proposed in this paper and integrated with a room temperature model. The main contributions of this paper are:

- Development of a 5kW/60kWh industrial-scale multi-physics and thermal VRFB model
  in Simulink/Matlab environment based on the stack configurations of an experimental
  5kW/3kWh VRFB system. It considers the reversible entropic heat, ohmic heat, selfdischarge heat and heat exchange from the electrolyte storage tanks and air.
- Comprehensive assessment of thermal dynamics of the VRFB system during charging/ discharging processes and their steady-state thermal impact after a long-time operation.
- Evaluation of the standby thermal behaviour of the VRFB system, which shows the importance of using a low cooling flow rate for electrolyte circulation to avoid thermal precipitation.
- Development of an integrated room temperature model that consists of the proposed VRFB
  thermal model with an active cooling mechanism by an air conditioner. The effectiveness
  of using an air conditioner for the thermal management of VRFB is examined by this

model.

Proposing an optimised cooling strategy based on the thermal behaviour of the entire system during the charging/discharging process to reduce the power consumption of the air conditioner by 48% while preventing thermal precipitation.

The rest of the paper is organised as follows. Section 2 introduces the multi-physics VRFB model and thermal modelling of VRFBs. In Section 3, simulation studies are carried out to investigate the influence of electrolyte flow rate, charging/discharging current and ambient temperature on the thermal dynamics of VRFBs. Also, standby thermal behaviours are studied in this section. Finally, an integrated room temperature model that consists of the proposed VRFB thermal model with an active cooling mechanism by an air conditioner is developed to investigate the thermal management of the VRFB system. Based on the conclusion drawn in Section 3, a centralised cooling strategy is proposed to optimise the air conditioner power consumption, validated in two case studies.

#### 2. Methods for battery model formulation

A schematic diagram of a typical VRFB system is given in Fig. 1. As a flow battery, the VRFB has hydraulic electrolyte circulation, unlike solid-state batteries. This makes the thermal dynamics of VRFB systems more complex. The electrolyte flows between the two storage tanks and the cells to allow chemical reactions to generate/absorb electrons for electrical energy usage/storage. Each cell is composed of two electrodes and has a membrane that separates the cell into the negative side and the positive side. The membrane is crucial to prevent the diffusion of vanadium ions which causes self-discharge reactions. Two pumps maintain the electrolyte circulation during operation to provide sufficient bulk concentration levels in the cell stack. The chemical reactions in positive/negative half-cells and overall cell reaction are shown as follows:

Negative half-cell:

$$V^{3+} + e^{-} \stackrel{\text{Charge}}{\rightleftharpoons} V^{2+} \quad E_N^0 = -0.255 \text{V}$$
 (1)

Positive half-cell:

$$VO^{2+} + H_2O \underset{\text{Discharge}}{\rightleftharpoons} VO_2^+ + 2H^+ + e^- \quad E_P^0 = 1.004V$$
 (2)

Overall cell:

$$VO^{2+} + V^{3+} + H_2O \underset{\text{Discharge}}{\overset{\text{Charge}}{\rightleftharpoons}} VO_2^+ + V^{2+} + 2H^+$$
 (3)

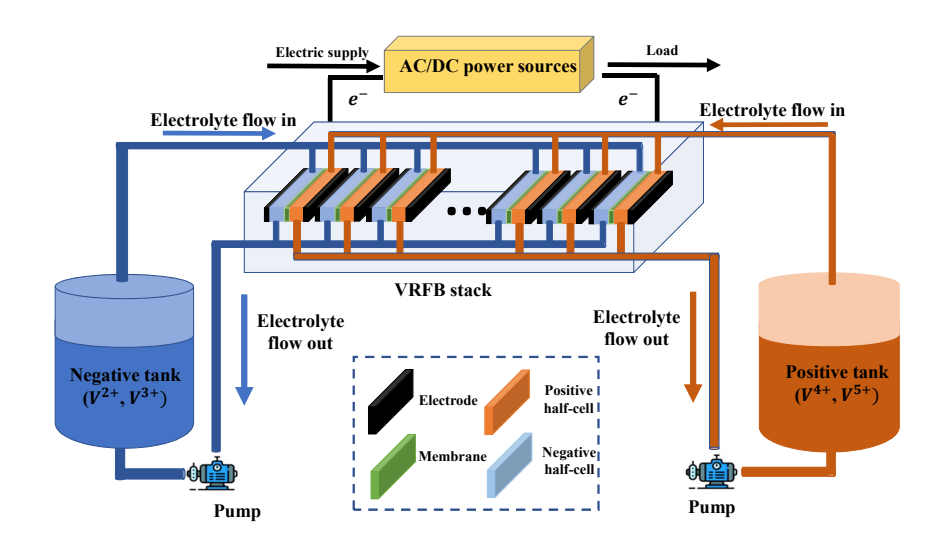


Figure 1: The typical structure and component of a VRFB system

To study the thermal dynamics of a VRFB system, an accurate thermal model is needed to reflect the electrolyte temperature variations in the battery stack and storage tanks. In this paper, a detailed integrated multi-physics model with thermal modelling of VRFBs is proposed to consider the overpotential heating, reversible entropic heating from chemical reactions, self-discharge reaction heating and the heating exchange by electrolyte flow rate and air. A multi-physics model, including an electrochemical model, has been commonly used to simulate the electrical dynamics of VRFBs via mass balance equations to simulate the vanadium species variations. In this study, the proposed thermal model is integrated with a multi-physics model to form an integrated multi-physics model with thermal modelling of VRFBs to investigate the thermal and electric behaviours of a large-scale VRFB system. This proposed VRFB model is

built in MATLAB/Simulink for battery simulation with the following assumptions:

- The initial temperature in the VRFB system is the same for different components [8].
- The electrolyte temperature and vanadium species concentration in each cell in the stack is uniform [6].
- The heat transfer of pipes and stack is neglected due to their minor heat exchange capabilities [6, 8, 10].
- The volume of electrolytes in each tank remains constant [8, 15].
- Gas evolution is not considered [8].
- The variation of the overall resistance of the stack is small and can be ignored [6].
- The effect of shunt current and related heat generation is minor and thus not considered in this study [6, 10].

## 2.1. Mass balance

The mass balance equations are adopted to quantify the cross-over of the vanadium ions in the battery stack. The variations of vanadium ions are caused by the cross-over phenomenon and the main chemical reactions in the charging/discharging process. Moreover, the vanadium ions in the stack are supplied from the two tanks by operating the two pumps for electrolyte circulation. The variation of the four oxidation states of the vanadium ions is affected by the electrolyte flow rate and chemical reactions in the stack. From the mass balance equations, the modelling of vanadium species variations can be given in the following equations as [8]:

For vanadium ions in the stack:

$$\frac{V_{stack}}{2} \frac{dc_2^s}{dt} = Q\left(c_2^t - c_2^s\right) \pm \frac{NI}{zF} - Nk_2 \frac{c_2^s}{D} S 
- 2Nk_5 \frac{c_5^s}{D} S - Nk_4 \frac{c_4^s}{D} S$$
(4)

$$\frac{V_{stack}}{2} \frac{dc_3^s}{dt} = Q\left(c_3^t - c_3^s\right) \mp \frac{NI}{zF} - Nk_3 \frac{c_3^s}{D} S 
+ 3Nk_5 \frac{c_5^s}{D} S + 2Nk_4 \frac{c_4^s}{D} S$$
(5)

$$\frac{V_{stack}}{2} \frac{dc_4^s}{dt} = Q\left(c_4^t - c_4^s\right) \mp \frac{NI}{zF} - Nk_4 \frac{c_4^s}{D}S 
+ 3Nk_2 \frac{c_2^s}{D}S + 2Nk_3 \frac{c_3^s}{D}S$$
(6)

$$\frac{V_{\text{stack}}}{2} \frac{dc_5^s}{dt} = Q\left(c_5^t - c_5^s\right) \pm \frac{NI}{zF} - Nk_5 \frac{c_5^s}{D} S - 2Nk_2 \frac{c_2^s}{D} S - Nk_3 \frac{c_3^s}{D} S$$
(7)

For vanadium ions in the tanks:

$$V_N \frac{dc_2^t}{dt} = Q\left(c_2^s - c_2^t\right) \tag{8}$$

$$V_N \frac{dc_3^t}{dt} = Q\left(c_3^s - c_3^t\right) \tag{9}$$

$$V_P \frac{dc_4^t}{dt} = Q\left(c_4^s - c_4^t\right) \tag{10}$$

$$V_P \frac{dc_5^t}{dt} = Q\left(c_5^s - c_5^t\right) \tag{11}$$

The parameters in the mass balance model have been shown in Tab. 1 with their definitions and values.

#### 2.2. Energy balance

In [8], the energy balance equations are developed to study the electrolyte temperature variations in different components of the VRFB system based on the energy conservation law. In the thermal model, the effect of heat generation, heat exchange and self-discharge reactions are considered, which allows a continuous simulation of the thermal dynamics of the VRFB system. In [6, 7], the heat generated from the active species self-discharge reactions is neglected to reduce

Table 1: VRFB model parameters and definitions used in this study

Symbol	Definition	Value
N	Number of cells in the stack	37
С	Total concentration of vanadium ions in mol L <sup>-1</sup>	1.5
$V_N$	Volume of the electrolyte in negative tank in L	1500
$V_P$	Volume of the electrolyte in positive tank in L	1500
$V_{stack}$	Volume of the stack in L	40
$H_e$	Height of the electrode in dm	3
$L_e$	Length of the electrode in dm	7
$W_e$	Width of the electrode in dm	0.025
S	Active area in dm <sup>2</sup>	21
d	Thickness of the membrane in dm	1.27e <sup>-3</sup>
T	Ambient temperature in K	298.15
R	Gas constant in Jmol <sup>-1</sup> K <sup>-1</sup>	8.314
ρ	Electrolyte density in kg m <sup>-3</sup>	1300
F	Faraday's constant in C mol <sup>-1</sup>	96,485
r'	Overall cell resistivity in Ω cm <sup>2</sup>	2.72
$k_2$	Diffusion coefficient of $V^{2+}$ in $m^2s^{-1}$	$8.768e^{-12}$
$k_3$	Diffusion coefficient of $V^{3+}$ in $m^2s^{-1}$	$3.222e^{-12}$
$k_4$	Diffusion coefficient of $V^{4+}$ in $m^2s^{-1}$	6.825e <sup>-12</sup>
k <sub>5</sub>	Diffusion coefficient of $V^{5+}$ in $m^2s^{-1}$	5.897e <sup>-12</sup>

the model complexity. In this study, the thermal model is adopted from [8, 9]. The electrolyte temperature in the stack,  $T_{\rm stack}$  is given by:

$$C_{p}\rho V_{\text{stack}} \frac{dT_{\text{stack}}}{dt} = Q_{P}C_{p}\rho \left(T_{P} - T_{\text{stack}}\right) + Q_{N}C_{p}\rho \left(T_{N} - T_{\text{stack}}\right) + I^{2}R_{\text{stack}} + IT_{\text{stack}}\frac{dE}{dT} + P_{\text{self-discharge}}$$

$$(12)$$

Here, the first two terms on the right side represent the heat exchange by the electrolyte flow rate,  $I^2R_{stack}$  is the heat generation by the overall stack resistance,  $IT_{stack}\frac{dE}{dT}$  is the reversible entropic heat generation within the stack, and  $P_{self-discharge}$  is the heat generation by the self-discharge reactions in the stack.

The open circuit voltage  $E^{OCV}$  of the VRFB system is given in terms of the standard electrode potential  $E^{\Theta}$  as:

$$E^{OCV} = E^{\Theta} + \frac{RT}{zF} \ln \left[ \left( \frac{c_{VO_2^+} c_{V^{2+}} c_{H^+}^2}{c_{VO_2^+} c_{V^{3+}}} \right) \left( \frac{\gamma_{VO_2^+} \gamma_{V^{2+}} \gamma_{H^+}^2}{\gamma_{VO_2^+} \gamma_{V^{3+}}} \right) \right]$$
(13)

In [9],  $E^{\Theta}$  is given as:

$$E^{\Theta} = -\frac{\Delta G^{\Theta}}{zF} = \frac{\Delta H_r^{\Theta} - T\Delta S_r^{\Theta}}{zF}$$
 (14)

where  $\Delta G^{\Theta}$  is the molar Gibbs free reaction enthalpy, and  $\Delta G^{\Theta}$  is represented by  $\Delta H_r^{\Theta}$  and  $\Delta S_r^{\Theta}$  for the molar reaction enthalpy and molar reaction entropy at the standard condition. Thus,  $\frac{dE}{dT}$  can be represented as:

$$\frac{dE}{dT} = \Delta S_r^{\Theta} + R \ln \left( \frac{c_{VO_2^+} c_{V^{2+}} c_{H^+}^2}{c_{VO^{2+}} c_{V^{3+}}} \right)$$
 (15)

Here,  $\Delta S_r^{\Theta}$  is the molar reaction entropy for the reactions. Due to the different reactants and products during the charging and discharging reactions, the main chemical reaction in the stack is a reversible entropic heat process. In the charging process, the main chemical reactions absorb heat; whereas in the discharging process, they produce heat. The derivations of  $\Delta S_r^{\Theta}$  are different in charging and discharging as:

For discharging:

$$\Delta S_r^{\Theta} = \sum S_{\text{products}} - \sum S_{\text{reactants}}$$

$$= S_{VO^{2+}} + S_{V^{3+}} + S_{H_2O} - S_{V^{2+}} - S_{VO_7^+} - 2S_{H^+}$$
(16)

For charging:

$$\Delta S_r^{\Theta} = S_{V^{2+}} + S_{VO_7^+} + 2S_{H^+} - S_{VO^{2+}} - S_{V^{3+}} - S_{H_7O}$$
(17)

Minor chemical reactions, such as the self-discharge reactions in the stack, will also cause additional heat generation. The self-discharge is caused by the diffusion of vanadium ions across the membrane, which reacts with other vanadium ions in another half-cell. The heat generation in the stack is presented as [8]:

$$P_{self-discharge} = N \cdot \left[ k_2 \frac{c_2^s}{d} S \cdot (-\Delta H_{(1)}) + k_3 \frac{c_3^s}{d} S \cdot (-\Delta H_{(2)}) + k_4 \frac{c_4^s}{d} S \cdot (-\Delta H_{(3)}) + k_5 \frac{c_5^s}{d} S \cdot (-\Delta H_{(4)}) \right]$$
(18)

where  $k_n$  is the diffusion coefficient,  $c_n^s$  is the molarity of each vanadium species in the stack,  $\Delta H_{(n)}$  is the changes of enthalpy for the different self-discharge reactions which are given in Eqs. (19)-(22). The thermodynamic dynamic parameters are listed in Tab. 2, noting that the enthalpy changes for the self-discharge reactions can be found in [8].

Table 2: Thermodynamic parameters for the reactants and products in the VRFB system, obtained from [8, 9]

Formula	State	$\Delta H_f^{\Theta}$ (kJ mol <sup>-1</sup> )	$\Delta S_f^{\Theta} \left( \text{J mol}^{-1} \text{ K}^{-1} \right)$
$V^{2+}$	Aqueous	-226.0	-130.0
$V^{3+}$	Aqueous	-259.0	-230.0
$VO^{2+}$	Aqueous	-486.6	-133.9
$VO_2^+$	Aqueous	-649.8	-42.3
$H_2 ilde{ m O}$	Aqueous	-285.8	69.9
$H^+$	Aqueous	0	0

$$V^{2+} + 2VO_2^+ + 2H^+ \to 3VO^{2+} + H_2O \tag{19}$$

$$V^{3+} + VO_2^+ \to 2VO^{2+} \tag{20}$$

$$VO^{2+} + V^{2+} + 2H^+ \rightarrow 2V^{3+} + H_2O$$
 (21)

$$VO_2^+ + 2V^{2+} + 4H^+ \rightarrow 3V^{3+} + 2H_2O$$
 (22)

The electrolyte temperature in the positive/negative tanks are:

$$C_p \rho V_p \frac{dT_p}{dt} = Q_p C_p \rho \left( T_{\text{stack}} - T_p \right) + U_{\text{tank}} A_{\text{tank}} \left( T_{\text{air}} - T_p \right)$$
 (23)

$$C_{p}\rho V_{N}\frac{dT_{N}}{dt} = Q_{N}C_{p}\rho \left(T_{\text{stack}} - T_{N}\right) + U_{tank}A_{\text{tank}} \left(T_{\text{air}} - T_{N}\right)$$
(24)

Please note that the thermal dynamics of the electrolyte in the two tanks are influenced by the heat exchange of the electrolyte from the stack and the overall heat exchange from the ambient air temperature and two tanks. The parameters in the VRFB thermal model have been given in Tab. 3 with definitions and values.

Table 3: Parameters and their definitions for the thermal model

Symbol	Definition	Value
$C_p$	Specific heat capacity of electrolyte in J g <sup>-1</sup> K <sup>-1</sup>	3.2
A <sub>tank</sub>	Surface area of the tank in $m^2$	9.8
$U_{\mathrm{tank}}$	Overall heat transfer capability of the tank in J K <sup>-1</sup> s <sup>-1</sup> m <sup>-2</sup> from [6]	3.67

#### 2.3. Multi-physics model

A multi-physics model is developed to combine these chemical laws with the electrical parameters, such as open circuit voltage (OCV), stack voltage, state of charge (SOC), etc. The OCV is defined as the voltage of a single battery cell without having any current flow, and the derivation of the OCV is formulated based on the Nernst equation as [15]:

$$E^{OCV} = E^{0'} + \frac{RT}{zF} \ln \left( \frac{c_2^s c_5^s}{c_2^s c_4^s} \right); E^{0'} = 1.40V$$
 (25)

Concentration overpotentials are an ineluctable part of the stack voltage, the derivation of these are learned from [16], which are different during the charging/discharging process:

$$\eta_{con}^{+} = \begin{cases} -\frac{RT}{zF} \ln(1 - \frac{I}{nFk_m L_e H_e c_s^3}), & \text{charging} \\ -\frac{RT}{zF} \ln(1 - \frac{I}{nFk_m L_e H_e c_s^3}), & \text{discharging} \end{cases}$$
(26)

$$\eta_{con}^{-} = \begin{cases} -\frac{RT}{zF} \ln(1 - \frac{I}{nFk_m L_e H_e c_s^2}), & \text{charging} \\ -\frac{RT}{zF} \ln(1 - \frac{I}{nFk_m L_e H_e c_s^2}), & \text{discharging} \end{cases}$$
(27)

Please note that in Eqs.(26)-(27),  $k_m$  is the mass transfer coefficient and is derived by the following equation from [16]:

$$k_m = 1.6 \times 10^{-3} \left( \frac{Q_c}{10 L_e W_e} \right)^{0.4} \tag{28}$$

The activation overpotentials ( $\eta_a^+$  and  $\eta_a^-$ ) are generally small compared with other overpotentials. As a result, the activation overpotentials are normally combined with the cell ohmic overpotential (ir) to form an overall cell ohmic overpotential (ir), which is:

$$ir' = ir + \eta_a^+ + \eta_a^-$$
 (29)

#### 2.4. The overall stack voltage

The stack voltage is expressed as the sum of the OCV, overall cell ohmic overpotential, and concentration overpotentials multiplied by the number of cells (N) from [16]:

$$E_{\text{stack}} = N(E^{OCV} + ir' + \eta_{con}^{+} + \eta_{con}^{-})$$
 (30)

The SOC of the VRFB system is defined as the average SOC level in the negative tank and positive tank:

$$SOC_N = \frac{c_{V^{2+}}}{c_{V^{2+}} + c_{V^{3+}}} \tag{31}$$

$$SOC_P = \frac{c_{VO_2^+}}{c_{VO_2^+} + c_{VO_2^{2+}}} \tag{32}$$

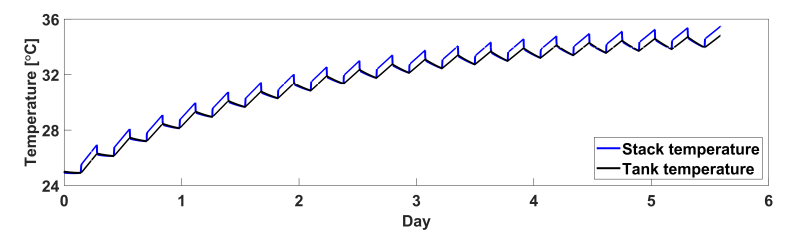
$$SOC = \frac{SOC_N + SOC_P}{2} \tag{33}$$

## 3. Simulation study on the thermal dynamics of a VRFB system

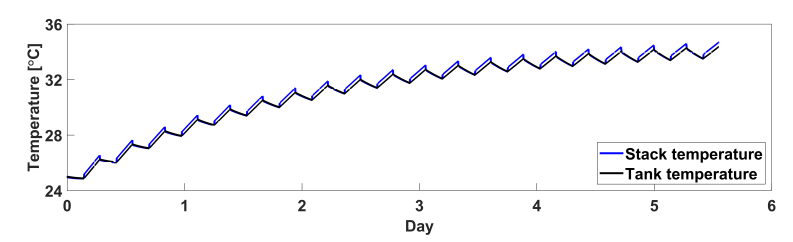
Based on the mass balance, energy balance and multi-physics models in Section 2 from [8], an integrated multi-physics VRFB model with thermal modelling is developed to investigate the performance of a 5kW/60kWh VRFB system, extended from a laboratory-scale 5kW/3kWh VRFB system with the same stack design. To investigate the thermal dynamics of VRFBs influenced by different factors, a simulation study is conducted, and further conclusions can be drawn from the analysis of the simulation results.

3.1. The influence of electrolyte flow rate, currents and ambient temperature on the electrolyte temperature in VRFB system

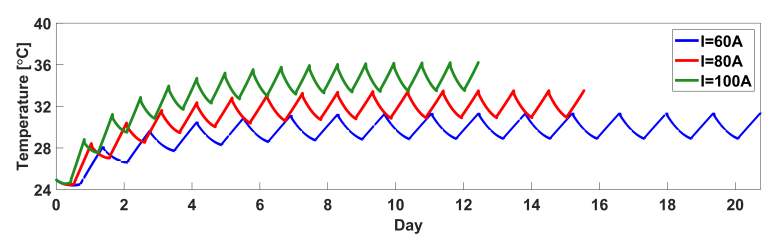
From the thermal modelling in Section 3, the heat generation during the battery charging/discharging cycles is from the battery stack in three main parts: ohmic overpotentials, self-



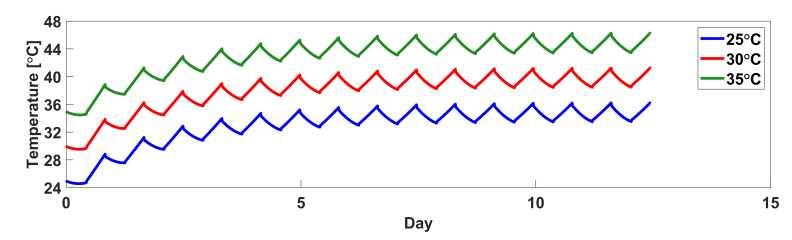
(a) Electrolyte temperature in the stack and tanks with a flow rate of 0.3L/s and constant current of 100A over 20 cycles at  $25^{\circ}$ C



(b) Electrolyte temperature in the stack and tanks with a flow rate of 0.6L/s and constant current of 100A over 20 cycles at  $25^{\circ}$ C



(c) Electrolyte temperature in the stack with constant currents of 60A, 80A and 100A at  $25^{\circ}$ C and a constant flow rate of 0.8L/s



(d) Electrolyte temperature in the stack with constant currents of 100A at  $25^{\circ}$ C,  $30^{\circ}$ C and  $35^{\circ}$ C and a constant flow rate of 0.8L/s

Figure 2: Simulation results of the electrolyte temperature in the stack and tank under different electrolyte flow rates, currents and ambient temperatures

discharge reactions, and reversible entropic heat during the discharging process. Two tanks are connected with the stack as a heat exchange source, contributing to the stack temperature reduction by exchanging the electrolyte. It is worth mentioning that in medium-scale or large-scale

VRFB systems, the VRFB stack is composed of 30-50 cells with a total volume much less than the total volume of electrolytes in the two tanks. The volume of tanks can be up to 500-2000L, hence a considerable heat exchange capability due to its large surface area. The heat generation in the VRFB system results in a temperature difference between the stack and tanks during the battery operation. As a result, the flow rate is one of the decisive factors influencing the electrolyte heat exchange capability in the VRFB stack.

In Figs. 2 (a) and (b), a simulation study is carried out to demonstrate the effect of flow rates on the thermal imbalance between the stack and tank. Here, the ambient temperature is set to be 25°C, and the initial electrolyte temperatures are assumed identical throughout the VRFB system components. The charging/discharging currents are 100A, and flow rates are set to 0.3L/s and 0.6L/s, respectively. Furthermore, to minimise the effect of self-discharge losses influenced by the flow rate, the SOC range is set to 40% to 60% over 20 cycles to show the thermal dynamics of this VRFB system. It was found that the electrolyte temperature in the stack and tanks in both figures increased gradually, reaching a steady state condition after about 15 cycles. It can be seen that the electrolyte temperature rapidly increases during the discharging process while decreasing during the charging process. The reason behind this is that the reversible entropic heating becomes negative during charging and positive during discharging, which absorbs generated heat during the charging process and generates heat during the discharging process. In Fig. 3, the heat absorption/generation in the stack with a 100A charging/discharging current is given. As seen in the figure, the reversible heat absorption is compensated by the large irreversible heat generation from overpotentials and self-discharge reactions during the charging process. During discharging, however, the reversible heat generation term is added to other heat generation sources and causes nearly 1500J/s of heat generation. Moreover, during the charging process after one day in Fig. 2 (a), the electrolyte temperature reduction is more evident due to the increase of temperature difference, providing sufficient heat exchange to cool the VRFB system naturally. This cannot be seen in the discharging process due to the large heat production in the stack. By comparing Figs. 2 (a) and (b), it can be concluded that a higher electrolyte flow rate reduces the electrolyte temperature difference from the stack to the tank. However, it has

no significant impact on the electrolyte temperature in the tank. The reason behind this is that the thermal dynamics of the VRFB system are determined by the heat generation in operation and the cooling from the ambient air. The control of the electrolyte flow rate is more effective in removing the heat accumulation in the stack and reducing its temperature, but not promising to cool down the whole VRFB system.

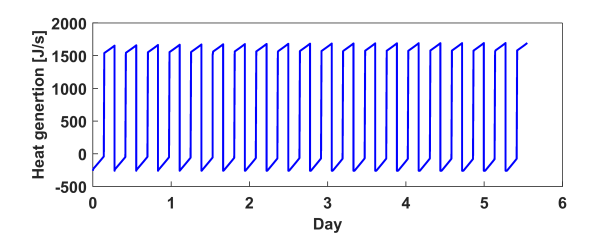


Figure 3: Heat absorption/generation under 100A charging/discharging current over 20 cycles

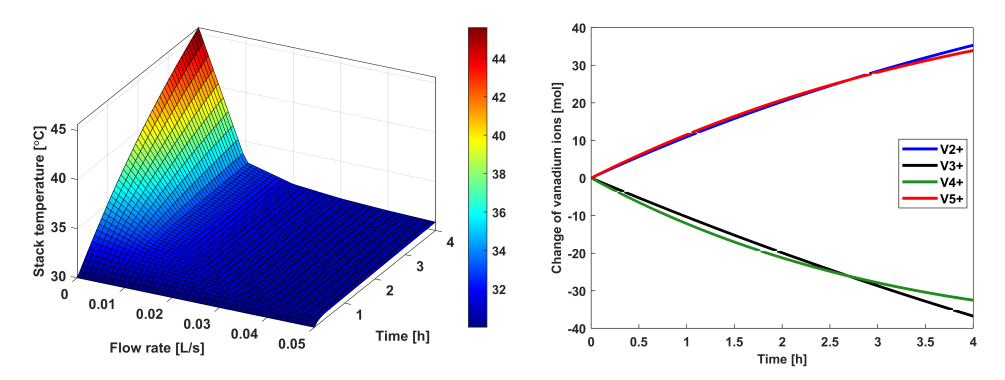
In the thermal modelling of VRFB systems, the heat generation is associated with the currents related to the three irreversible heat generation mechanisms. Meanwhile, the ambient temperature influences the heat exchange of the VRFB system. Therefore, to investigate the significance of current on the thermal dynamics of the VRFB system, another simulation study is carried out in this paper to study the electrolyte temperature in the stack under 60A, 80A, and 100A charging/discharging currents at 25°C ambient temperature during 15 cycles, with the electrolyte flow rate at 0.8L/s. The SOC range, in this case, is from 20% to 80%. In Fig. 2 (c), it is clear that a higher current will lead to a higher electrolyte temperature rise in the stack due to more irreversible heat generation. Another simulation result is shown in Fig. 2 (d), showing the electrolyte temperature in the stack with 100A charging/discharging current under 25°C, 30°C and 35°C ambient temperature over 15 cycles. The electrolyte temperature variations in the stack have a nearly identical pattern, but it is clear that a higher ambient temperature produces a higher steady-state electrolyte temperature in the stack. Moreover, with an ambient temperature of 35°C, after two days, the electrolyte temperature exceeded 40°C and remained above this value. As mentioned in the previous section, this makes thermal precipitation that threats the safe operation of a VRFB system. This result highlights the necessity to conduct active cooling control for thermal management. Fig. 2 (c) shows that by limiting the discharging current, the electrolyte

temperature can be decreased to a lower level in the steady-state condition. However, considering the fact that satisfying customers' demand is the primary objective in most applications, efficient cooling strategies are necessary for real-world applications where the VRFB is coupled with a microgrid or other in a residential premise with generation and storage units.

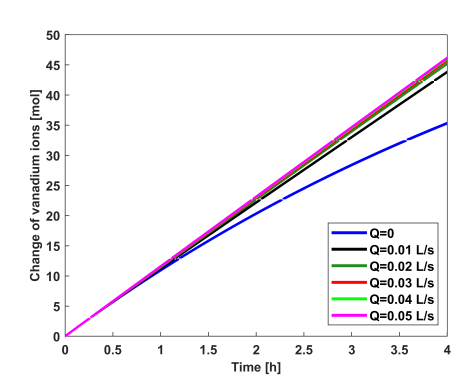
#### 3.2. Standby thermal behaviours

In [8], Tang et al. carried out a simulation to study the thermal behaviour of a kW-level VRFB system over a one-day period. The study showed a significant rise in the temperature of the stack when the whole VRFB system was left idle. The temperature rise stems from the self-discharge reactions when no current is applied to a VRFB system that produces heat within the stack. The generated heat will be accumulated because there is no pump operation to maintain electrolyte circulation within the VRFB system, as it is common to turn off the pump in idle mode. In [7], Trovo et al. conducted a detailed study to investigate the standby thermal behaviour of an industrial-scale VRFB system. The authors concluded that a higher SOC level during the standby period caused more heat generation by self-discharge reactions. They discovered that when the initial SOC was 95%, the maximum temperature in the stack went up to  $60^{\circ}$ C, which is highly likely to cause thermal precipitation of  $V_5^+$ . To prevent this, a cooling flow rate is necessary.

In this section, the standby thermal dynamics of a VRFB system are investigated to demonstrate the effect of a cooling electrolyte flow rate in the standby period. In Fig. 4 (a), the variations of the electrolyte temperature in the stack are shown over time under different constant electrolyte flow rates under an ambient temperature of 30°C with an initial SOC of 80%. As can be seen from this figure, if there is no flow rate for electrolyte circulation, after 4 hours, the electrolyte temperature in the stack exceeds 45°C. With a flow rate of over 0.02L/s, the heat generation from the self-discharge reactions in the stack can be effectively transferred into the electrolyte tank, preventing a significant electrolyte temperature increase within the stack. Moreover, in Fig. 4 (b), the change in the amount of four oxidation state vanadium ions is given when there is no electrolyte flow rate. It is clear that the amount of  $V_2^+$  and  $V_5^+$  ions are increasing and the amount of  $V_3^+$  and  $V_4^+$  ions are decreasing in this period. This is caused by the cross-over phenomenon of vanadium species diffusing across the membrane and self-reacting with each other. These self-



(a) Electrolyte temperature in the stack vs. flow rates and (b) Change of vanadium species of the VRFB system vs. time with no electrolyte flow rate



(c) Molar losses of active species in the VRFB system over 4 hours vs. time for different flow rates

Figure 4: Simulation results in standby mode showing the effect of the flow rate at 80% initial SOC

discharge reactions lead to the capacity fading of a VRFB system. Also, the electrolyte flow rate will cause a difference in the capacity fading due to the concentration level of vanadium species in the stack supplied from the tank. To study the electrolyte flow rate effect on the capacity fading, a new simulation study was carried out, the results of which are shown in Fig. 4 (c). It can be seen that when there is zero electrolyte flow rate in the VRFB system, the molar losses are the smallest, around 33mol in 4 hours. Moreover, the molar losses under the other five different electrolyte flow rates show almost no change, only 11mol higher than the zero electrolyte flow rate. The reason behind this is that the electrolyte flow rate constantly supplies vanadium ions from the tank to the stack, thus accelerating the vanadium species diffusion leading to more

molar losses.

Considering the standby thermal behaviour of the VRFB system, a low electrolyte flow rate is needed for stack electrolyte cooling for the 5kW/60kWh VRFB to prevent thermal precipitation during the standby mode. Here, we assume that the minimum pump speed is 0.05L/s, which is used for standby cooling. Considering the modelling result of pump speed vs. flow rate given in [17], an electrolyte flow rate lower than 0.1L/s achieves a low total pump power consumption of around 10W. This result indicates the effectiveness of utilising pumps for standby cooling without using a significant amount of energy in this case study. However, for different VRFB systems with different pump designs and configurations, such a low flow rate may not be achievable in practice. As a recommendation, a low flow rate with minor pump power consumption can be used for electrolyte circulation during the standby mode to prevent thermal precipitation in the stack.

#### 4. Case studies and results of air flow cooling for a VRFB system

In most battery technologies, active or passive cooling strategies, e.g., by natural air flow or forced air cooling using fans in the battery stack, are popular solutions to regulate battery cell temperature, as reported in [18]. Moreover, in [19], the authors concluded that an effective cooling system is important to prevent thermal runaway, which is responsible for the safe operation of a battery system. Air cooling fans and other advanced integrated cooling systems are commonly used for solid-state batteries in EVs and other applications, as mentioned in [20, 21, 22]. The VRFB stack contains liquid electrolytes with small channels, and a well-designed VRFB stack has to be isolated from the air to prevent the oxidation of vanadium ions. As a result, the use of air-cooling fans inside the stack is impossible for VRFBs. For the thermal management of VRFBs, a limited number of paper has addressed the issue of efficient thermal management to prevent thermal precipitation. In [9], a shell and tube heat exchanger is designed to cool down the electrolyte as it moves out of the stack and shows promising results in simulation. However, the results do not establish the effectiveness of using the proposed heat exchanger is not vali-

dated to show its applicability and effectiveness in commercial VRFB systems. Another efficient thermal management system by flow rate control is presented in [6]. Although the electrolyte temperature and system efficiency are significantly improved by the optimised flow rate control method proposed in that paper, the electrolyte flow rate control does not guarantee effective thermal management over long operational cycles, and a cooling system is still essential to provide sufficient heat exchange for VRFB systems. In [2], a standby thermal management system is designed to have a low electrolyte flow rate to dissipate the cross-over heat generation in the stack. Nevertheless, only the thermal management method during the standby period is investigated in that study, neglecting the thermal management during operation.

Considering the fact that most of the industrial-scale VRFB systems are relatively large, the heat accumulation during the charging/discharging processes is relatively slow compared to other battery technologies. Also, the thermal precipitation of vanadium species is sensitive to temperature rise in the long term. Thus, a VRFB does not require a high-capacity cooling system to rapidly reduce its temperature but the prevention of electrolyte temperature going over safe limits over hours and days is necessary. As a result, a common air conditioner unit could be sufficient for the thermal management of VRFBs. For instance, the Roseworthy solar farm and energy storage site at the University of Adelaide, Australia, has 14 individual VRFB systems operating in a room equipped with an air conditioner to cool down the room temperature [23]. For these 14 commercial VRFB systems, due to the lack of an integrated cooling mechanism within them, active temperature control using an air conditioner is used to ensure its operational stability, as mentioned in [14]. As for the thermal management of the VRFB, the objective is to prevent the electrolyte temperature in the stack from exceeding 40 °C [6, 7, 9]. To investigate the feasibility of using a standard air-conditioner for efficient thermal management of VRFBs, a room temperature model considering a simplified air-conditioning system model is presented in this paper. The goal is to study the effect of active temperature control in reducing the electrolyte temperature in the VRFB system.

## 4.1. A room temperature model considering a simplified air-conditioning unit model

To investigate the thermal dynamics of a VRFB system in the presence of an active cooling system, a thermal model of a room is adapted from [24, 25]. The thermal model considers the dynamics of ambient air temperature outside the building while taking the heat exchange of the VRFB system and the characteristics of the air-conditioner into account. The formulation of the integrated room temperature model is as follows:

$$\frac{dQ_{cool}(t)}{dt} = (T_{room} - T_{ac}) \cdot M_{dot} \cdot C \tag{34}$$

$$\frac{dQ_{loss}(t)}{dt} = (T_{out} - T_{room}) \cdot h \cdot A_{wall}$$
(35)

$$\frac{dT_{room}(t)}{dt} = \frac{1}{M_{air} \cdot C} \cdot \left( \frac{dQ_{loss}}{dt} + \frac{dQ_{heat}}{dt} - \frac{dQ_{cool}}{dt} \right)$$
(36)

Eq. (34) is the air flow cooling model of the air-conditioner, and Eq. (35) is the heat losses caused by the heat exchange from the outside temperature to the walls. Eq. (36) is the overall room heat exchange equation, influenced by the heat losses from outside air, heat generation from the VRFB system and heat exchange from the air. The room temperature model is developed based on the following basic assumptions:

- The dimensions of the room are  $5m \times 4m \times 3m$  assuming that every wall, floor and roof are made of normal 0.2m thick concrete.
- The temperature of the ground is assumed to be the same as the air temperature.
- Except for the VRFB system, there is no other heat source inside the room.
- The control of the air conditioner is realised by adjusting the air flow temperature. The air mass flow of the air conditioner is constant.
- The initial air temperature in the room is 25°C, while the total air volume in this room equals its volume.

All of the parameters of the integrated room temperature model are given in Table 4. The air conditioner has a 3kW cooling capacity, and the rated electrical input power is 1kW. Assume the air conditioner has no standby power consumption, the power consumption of the air conditioner in cooling mode is calculated by:

$$P_{ac}(t) = \frac{dQ_{cool}(t)}{dt} / EER \tag{37}$$

Here, the *EER* is the Energy Efficiency Ratio, defined as the ratio of the cooling provided by the air conditioner unit to its input power consumption.

Table 4: Thermal parameters of the integrated room thermal model

Symbol	Definition	Value
$A_{wall}$	Total surface of walls in m <sup>2</sup>	94
h	Heat transfer coefficient of concrete in W m <sup>-2</sup> K <sup>-1</sup>	5.32
$M_{dot}$	Air mass flow through air conditioner in kg h <sup>-1</sup>	1500
C	Heat capacity of air in J kg <sup>-1</sup> K <sup>-1</sup>	1020
Mair	Air mass inside the room in kg	121
EER	Energy efficiency ratio	3

## 4.2. Case study 1: Thermal dynamics of a VRFB system without active air flow cooling

To investigate the thermal dynamics of an industrial-scale VRFB system without active cooling, the developed thermal model of the VRFB and the integrated room temperature model are combined in this case study. It is assumed that the VRFB system is stored in a small room (see Fig. 6), as mentioned in the previous section, and connected to a grid that purchases electricity from the grid when battery energy is not enough to cover the load. When excess PV generation is available, or the grid electricity is cheap, the battery is charged to release at the time of need (mainly at night). Assume the battery is charged at a constant rate from 7AM to 6PM daily in the 15 days of simulation. The charging current is 100A (about 5kW) throughout the charging period until the SOC of the VRFB system reaches 80%. Then after 7 PM each day, assume a high electrical energy demand, requiring a discharging current of 100A, is supplied by the VRFB until its SOC reaches 20%. The VRFB system will go into standby mode if there are no charging/discharging activities after reaching the SOC limits. To prevent the thermal precipitation of

the vanadium species in the stack during the standby period, a constant flow rate of 0.05L/s is applied for cooling. To simulate efficient operation with respect to pump power consumption, an optimised electrolyte flow rate control method – the variable flow rate from [26] – is used to dynamically control the flow rate and minimise losses. The formulation of the variable flow rate is given in Eqs. (38)-(39).

$$Q = N \cdot FF \cdot \frac{|I|}{nFc(1-SOC)}, \quad \text{charging}$$
 (38)

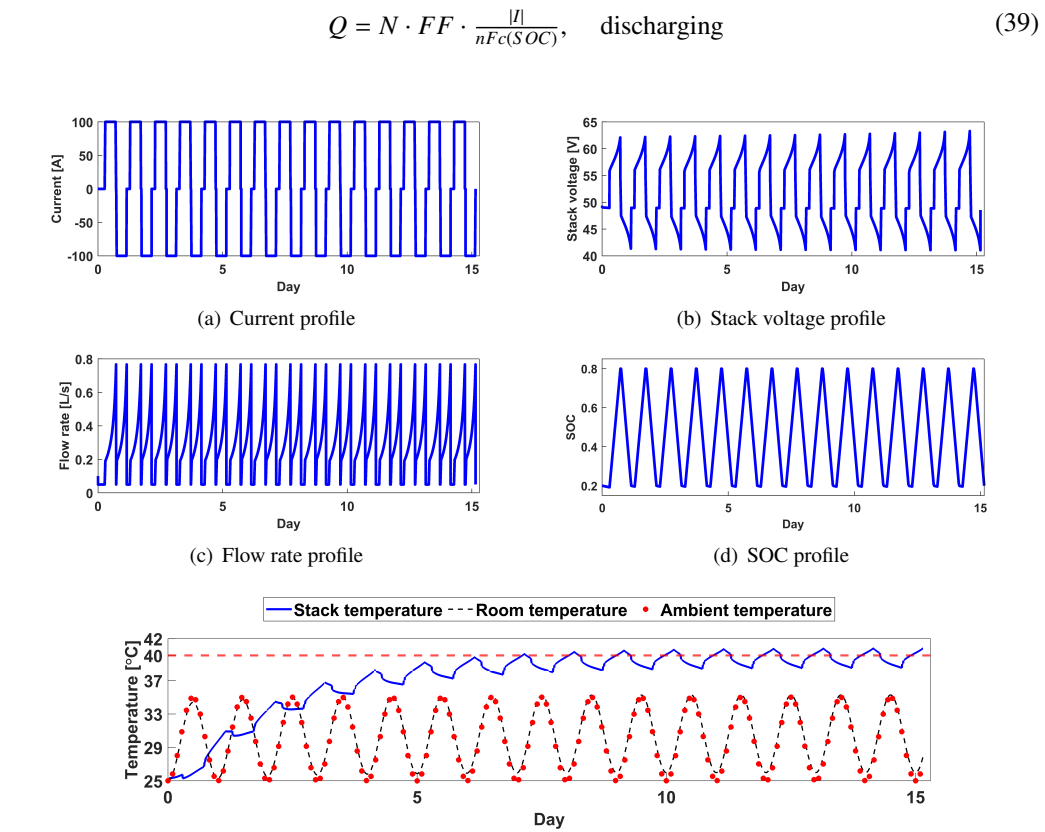


Figure 5: Case study 1: Without active cooling mechanism - Simulation profiles of 5kW/60kWh VRFB system over 15 days

(e) Temperature profiles

Here, FF is the fixed stoichiometry flow factor normally considered constant. For this VRFB

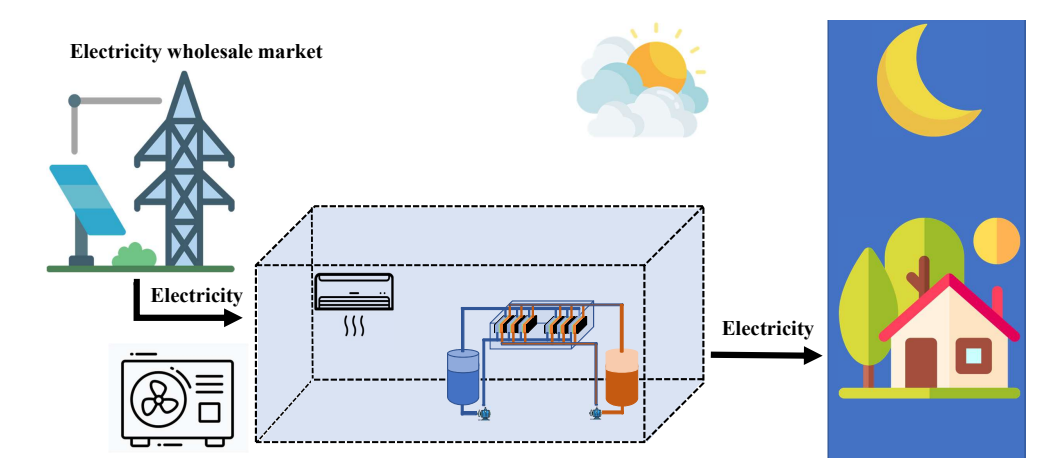


Figure 6: A residential application of VRFB during daytime and night time

system, the FF is chosen as 6 for 100A current to achieve a more balanced performance in system energy efficiency and capacity in high current applications compared with a constant flow rate. As a result, in this study, the flow rate control is realised using the variable flow rate control method of FF=6, and the pump speed range is from 0.05L/s to 0.8L/s.

A 15-day simulation is carried out considering a varying daily ambient air temperature from 25°C to 35°C in a sinusoidal fashion, as suggested in [8]:

$$T_{\text{air}} = (T_{\text{max}} - T_{\text{min}}) \cdot \sin^2(\omega t + \varphi) + T_{\text{min}}$$
(40)

In Eq. (40),  $T_{\rm min}$  and  $T_{\rm max}$  stand for the minimum/maximum ambient air temperature within a day. Also,  $\omega$  and  $\varphi$  are the angular frequency and phase, their units are rad/s and rad, respectively. It is assumed that the lowest temperature is at midnight; thus, the phase in Eq. (40) can be derived based on this assumption.

In Fig. 5 (a), the VRFB current for the 15 days is shown. As indicated earlier, the charging/discharging current is constant at 100A throughout the operation. The standby period is also shown in this figure when there is no current flow into/out of the VRFB system. The stack voltage profile is shown in Fig. 5 (b), and the electrolyte flow rate profile is presented in Fig. 5 (c). Under FF=6, the flow rate varied from 0.16L/s to 0.76L/s and dynamically changed with the

SOC of the VRFB system. The SOC profile in Fig. 5 (d) shows that the standby mode will lead to minor stored energy loss due to self-discharge. Considering the range of SOC from 20% to 80%, it can be neglected safely. Most importantly, the outside air temperature, electrolyte temperature in the stack and room temperature profiles are given in Fig. 5 (e). It can be seen that the room temperature follows the outside air temperature when there is no active cooling mechanism in place. Moreover, the electrolyte temperature in the stack has an overall increasing trend in these 15 days and reaches the steady-state condition almost after 10 days. Similar to the results mentioned in the previous section, the electrolyte temperature in the stack decreases during the charging process due to the reversible entropic heating during the daytime. Note that the outside air temperature during the charging process from 7 AM to 6 PM is higher than 30°C in the 15 days. This highlights that it is unnecessity to use an active cooling strategy during the charging process if the outside air temperature is not very high. Nevertheless, the results in Fig. 5 (e) show that the electrolyte temperature in the stack increases significantly during the discharging process. On day 7, the electrolyte temperature exceeded 40°C for the first time, with 9 hours above the 40°C recommended threshold on the eighth day. In [2, 6, 8], the safe operating electrolyte temperature is defined as 10-40 °C to prevent the capacity fading, stack channel congestion and membrane damage caused by the thermal precipitation of vanadium ions. In this case, nearly 9 hours of high electrolyte temperatures in the stack will threaten the stability and reliability of the VRFB system. Considering the role of a VRFB system in an off-grid application, where continuous operation is required over a long period of time, the necessity of safe and efficient management of the electrolyte temperature becomes more apparent.

#### 4.3. Case study 2: Thermal dynamics of a VRFB system with active cooling mechanism

As mentioned in the previous section, active cooling is necessary to maintain the electrolyte temperature below the threshold over a long operational period to prevent thermal precipitation and related consequences. However, most current VRFB system designs do not contain an active cooling mechanism, including air flow or liquid cooling systems. Thus, in most on-site applications of VRFBs, using air conditioners to realise air flow cooling has become the primary solution for thermal management. In this case study, the feasibility of using air conditioners

to manage the thermal dynamics of an industrial-scale VRFB system is investigated, where the same operational conditions and profiles are used from case study 1.

In this case study, an air conditioner ensures the room temperature remains below 30°C to provide sufficient heat exchange for the VRFB system. That results in the electrolytes in the tank being adequately cooled down, and thus the electrolyte transferred from the tanks to the stack is cooler, contributing to decreasing the overall electrolyte temperature in the stack. The temperature profile of the cooling mechanism is given in Fig. 7 (a). Here, it is clear that the room temperature has been kept below 30°C after the first six days when the outside air temperature is higher. Note that there is no active cooling in the first six days because there is no thermal precipitation issue. Moreover, when the outside air temperature is lower than 30°C, the air conditioner is turned off. The result is that after 15 days of operation with 15 charging/discharging cycles, the electrolyte temperature in the stack does not exceed the 40°C of thermal precipitation level, where the highest temperature is 39.8°C. This case study proves the effectiveness of using an active air cooling mechanism to offer effective thermal management for VRFB systems.

Here, we proposed an improved operational strategy for managing heat in a VRFB system. As shown in the results and discussions given in Fig. 2 (c) and (d) and Section 3, there is almost no heat generation in the stack during the charging process due to the reversible entropic heating. As a result, if there is no extreme weather condition with an ambient temperature higher than 40°C that lasts more than several hours, it is unnecessary to operate an active cooling device to protect VRFB against thermal precipitation caused by excessive heat. This is because the main chemical reactions will absorb heat during the charging process and hence decrease the electrolyte temperature within the stack. However, when the discharging process starts, significant heat will be produced, leading to a rapid increase of the electrolyte in the stack; thus, an active cooling strategy is necessary to ensure a sufficient heat exchange. As a result, an improved cooling strategy could be to turn off the cooling system during the charging process in the daytime and utilise a lower room temperature limit of 25°C during the discharging process at night time. The reason for using a lower room temperature limit in this period is to provide sufficient heat

exchange for the VRFB system, as the exchange amount is proportional to the integration of the temperature difference over a specific period.

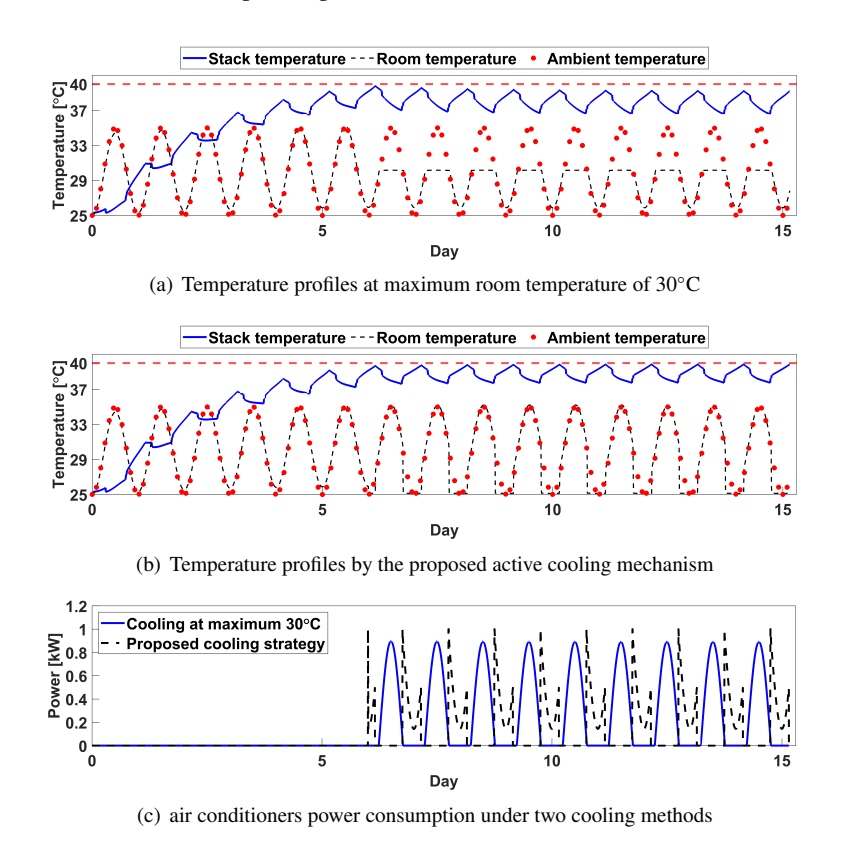


Figure 7: Case study 2: With active cooling mechanism - Simulation results for 15 days with a varying ambient temperature ranging from  $25^{\circ}C$  to  $35^{\circ}C$ 

The simulation results of the proposed improved cooling strategy are given in Fig. 7 (b), where the electrolyte temperature in the stack is kept below 40°C to prevent thermal precipitation. In both cases, the cooling actions were carried out only after six days because there was no thermal precipitation problem within the first six days. It is interesting to note that this approach results in a lower stack temperature variation. Furthermore, the simulation results of the air conditioner power consumption are given in Fig. 7 (c), which shows that these two cooling strategies operated during different periods of the charging/discharging process. The power consumption is 64.2kWh by constant temperature cooling of 30°C, while it is reduced to 33.4kWh by the pro-

posed optimised cooling strategy at 25°C during the discharging processes. This result shows that operating the cooling system during the discharge process can be more energy-efficient for VRFB systems, and the energy-saving could be up to 48% in this case.

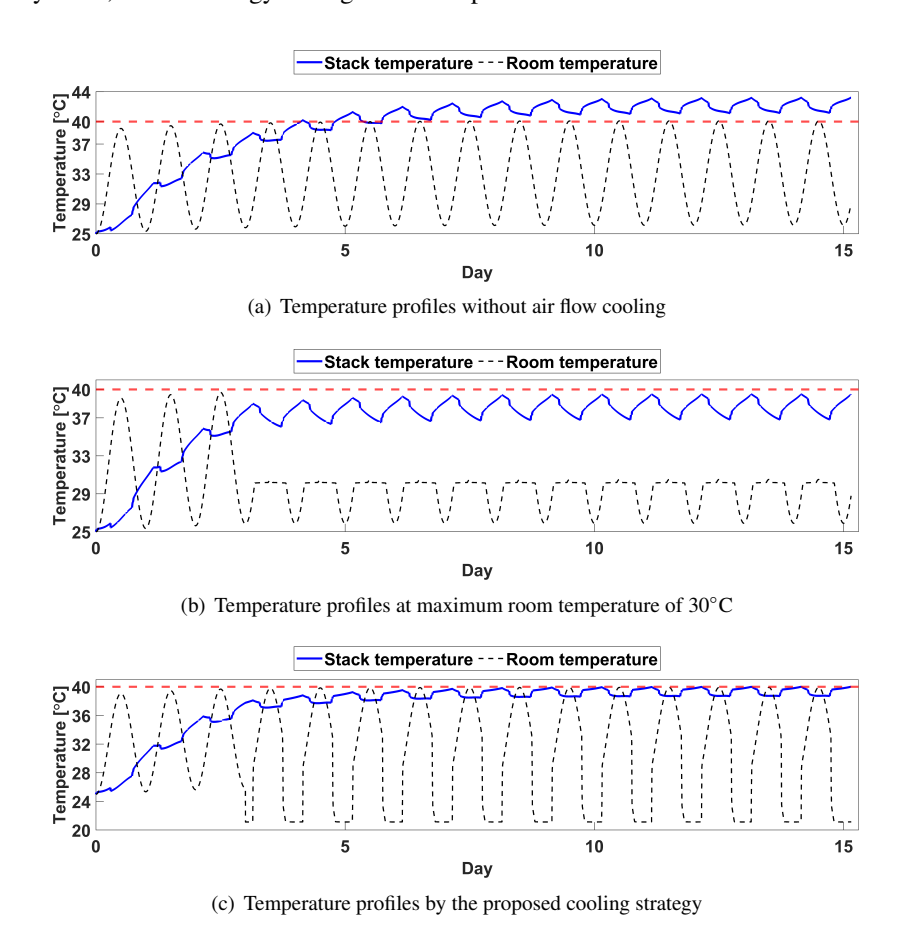


Figure 8: Simulation results of 15 days with and without cooling with a varying ambient temperature ranging from  $25^{\circ}\text{C}$  to  $40^{\circ}\text{C}$ 

In some areas, e.g., Australia, daytime temperature above 35°C is common during summer, which may easily lead to the electrolyte temperature in the stack exceeding 40°C at steady-state, rather than going up and down during the charging/discharging processes, as shown in Fig. 5 (e). Moreover, a higher ambient temperature requires more power consumption from the air conditioner. Thus, another case study is examined to explore the cooling requirements with an outdoor air temperature varying between 25-40°C using Eq. (40). Other basic consumption and

operational conditions (e.g. SOC limits, charging/discharging currents, cooling electrolyte flow rate etc.) remain the same as in previous case studies. Due to the higher ambient temperature in this study, the maximum cooling capacity of the air conditioner is raised to 5kW, and the rated cooling input power is increased to 1.7kW, correspondingly. The simulation results of the electrolyte temperature in the stack and room temperature profile with no active cooling mechanism, constant cooling strategy and the proposed cooling strategy are given in Fig. 8 (a)-(c). Note that the active cooling mechanism in both cases started operating only after the third day for the same reasons mentioned before. It can be seen from Fig. 8 (a) that without any active cooling action, the electrolyte temperature in the stack increased to 40°C after five days and exceeded the safe limit throughout the next ten days. The use of a constant 30°C maximum daytime cooling strategy is shown in Fig. 8 (b), where the air conditioner consumed 190.6kWh in 15 days. Alternatively, the results of using a 21°C minimum night-time cooling strategy are given in Fig. 8 (c), which reduced the total air conditioner consumption to 139.6kWh without compromising the electrolyte temperature. This equates to a 27% of energy saving over the course of the simulation. These results highlight the necessity of developing effective thermal modelling of the VRFB and combining this with an integrated room temperature model considered the active air flow cooling to study the thermal dynamics of VRFB systems. This allows valuable insights into the VRFBs' thermal management that could lead to new cooling system design and operation strategies.

# 4.4. Recommendations for the future smart thermal management system development for VRFB systems by air flow cooling strategy

In this paper, an air flow cooling mechanism using an air conditioner for a large VRFB system is studied, which is practical for effective thermal management in real-world applications. Moreover, these developed models can advise the designers and operators of VRFBs on the thermal dynamics and required cooling strategies for these devices. Although the proposed optimised cooling strategy shows promising results in energy saving, in practice, the charging/discharging powers fluctuate in time due to solar PV generation and customer demands, etc., which is a different situation from the two case studies presented in this paper. Also, the variations of the

ambient temperature, albeit slow, are another challenge to performing efficient thermal management to minimise the power consumption of the cooling system. Thus, sophisticated cooling controllers must account for all variations and uncertainties. Until now, no efficient and validated smart cooling control system has been studied for VRFBs to minimise the cooling losses for thermal management. Therefore, a future research direction could be investigating the application of optimal and nonlinear controllers and optimisation to regulate cooling system operation. These proposed controllers and optimisation methods can be adjusted to different VRFB systems to fulfil different thermal management objectives, which is beneficial for the thermal management of VRFB in large-scale energy storage units under high-current charging/discharging regimes.

For the future development of an online smart room temperature control of a VRFB system, the cost function must minimise the total losses of the pump power consumption, concentration overpotential and cooling devices power consumption to obtain the optimal electrolyte flow rate and room temperature at each time step. Depending on the dynamics of demand, PV generation, ambient temperature etc., the time step length can vary, where a higher fluctuation will require a faster re-optimization.

#### 5. Conclusion

In this paper, a dynamic multi-physics VRFB model with an emphasis on the thermal dynamics of the technology is developed to investigate the thermal behaviours of a 5kW/60kWh VRFB system over a multi-day operation. The impact of electrolyte flow rate, current and ambient temperature on the thermal dynamics and steady-state performance of the VRFB system have been investigated. Moreover, the standby thermal behaviour of a VRFB system is studied. It is shown that the heat accumulation during the standby mode, caused by the self-discharge reactions, is significant and requires a mandatory, low electrolyte circulation flow to remove the heat from the battery stack. Finally, an active air flow cooling strategy using air conditioners is presented based on the insights from earlier simulation studies. The results proved the effectiveness of using air conditioners to manage heat within VRFB components. Most importantly, considering the different thermal behaviours of VRFBs during the charging/discharging process, a cooling

strategy is proposed to optimise the power consumption of the cooling unit. Two case studies are presented to show that compared with a constant maximum cooling temperature, the proposed strategy can reduce cooling power consumption by 48% in 15 days of operation.

To further improve the performance of the cooling system, a future direction of this research could focus on developing an intelligent room temperature control system to handle the impact of varying ambient temperatures. The VRFB system's internal states and external parameters could be used in the smart control system. Additionally, historical or simulation data can be used to train accurate artificial intelligence models (e.g., neural networks) to improve the decision-making process.

### Acknowledgment

Funding through a PhD scholarship is provided by the Microgrid Battery Deployment project, which is funded by the Future Battery Industries Cooperative Research Centre as part of the Commonwealth Cooperative Research Centre Program, Australia.

#### References

- [1] M Kazacos, M Cheng, and M Skyllas-Kazacos. Vanadium redox cell electrolyte optimization studies. *Journal of Applied electrochemistry*, 20(3):463–467, 1990.
- [2] Andrea Trovò and Massimo Guarnieri. Standby thermal management system for a kw-class vanadium redox flow battery. *Energy Conversion and Management*, 226:113510, 2020.
- [3] Nadeem Kausar, Asem Mousa, and Maria Skyllas-Kazacos. The effect of additives on the high-temperature stability of the vanadium redox flow battery positive electrolytes. *ChemElectroChem*, 3(2):276–282, 2016.
- [4] Donghyeon Kim and Joonhyeon Jeon. A high-temperature tolerance solution for positive electrolyte of vanadium redox flow batteries. *Journal of Electroanalytical Chemistry*, 801:92–97, 2017.
- [5] Shuibo Xiao, Lihong Yu, Lantao Wu, Le Liu, Xinping Qiu, and Jingyu Xi. Broad temperature adaptability of vanadium redox flow battery—part 1: Electrolyte research. *Electrochimica Acta*, 187:525–534, 2016.
- [6] Ankur Bhattacharjee and Hiranmay Saha. Development of an efficient thermal management system for vanadium redox flow battery under different charge-discharge conditions. *Applied Energy*, 230:1182–1192, 2018.
- [7] Andrea Trovo, Alberto Saccardo, Monica Giomo, and Massimo Guarnieri. Thermal modeling of industrial-scale vanadium redox flow batteries in high-current operations. *Journal of Power Sources*, 424:204–214, 2019.

- [8] Ao Tang, Jie Bao, and Maria Skyllas-Kazacos. Thermal modelling of battery configuration and self-discharge reactions in vanadium redox flow battery. *Journal of Power Sources*, 216:489–501, 2012.
- [9] Zhongbao Wei, Jiyun Zhao, Maria Skyllas-Kazacos, and Binyu Xiong. Dynamic thermal-hydraulic modeling and stack flow pattern analysis for all-vanadium redox flow battery. *Journal of Power Sources*, 260:89–99, 2014.
- [10] Bahman Khaki and Pritam Das. Parameter identification of thermal model of vanadium redox batteries by metaheuristic algorithms. *Electrochimica Acta*, 394:139131, 2021.
- [11] Zhongbao Wei, Jiyun Zhao, and Binyu Xiong. Dynamic electro-thermal modeling of all-vanadium redox flow battery with forced cooling strategies. *Applied energy*, 135:1–10, 2014.
- [12] Weixiong Wu, Shuangfeng Wang, Wei Wu, Kai Chen, Sihui Hong, and Yongxin Lai. A critical review of battery thermal performance and liquid based battery thermal management. *Energy conversion and management*, 182:262– 281, 2019.
- [13] Jiayuan Lin, Xinhua Liu, Shen Li, Cheng Zhang, and Shichun Yang. A review on recent progress, challenges and perspective of battery thermal management system. *International Journal of Heat and Mass Transfer*, 167:120834, 2021
- [14] Emil Holm Kirk, Filippo Fenini, Sara Noriega Oreiro, and Anders Bentien. Temperature-induced precipitation of  $v_2o_5$  in vanadium flow batteries—revisited. *Batteries*, 7(4):87, 2021.
- [15] Yifeng Li, Maria Skyllas-Kazacos, and Jie Bao. A dynamic plug flow reactor model for a vanadium redox flow battery cell. *Journal of Power Sources*, 311:57–67, 2016.
- [16] Yifeng Li. Advanced Modelling, Optimisation and Control of Vanadium Redox Flow Battery. PhD thesis, The University of New South Wales, 2018.
- [17] Md Parvez Akter, Yifeng Li, Jie Bao, Maria Skyllas-Kazacos, and Muhammed Fazlur Rahman. Optimal charging of vanadium redox flow battery with time-varying input power. *Batteries*, 5(1):20, 2019.
- [18] Heesung Park. A design of air flow configuration for cooling lithium ion battery in hybrid electric vehicles. *Journal of power sources*, 239:30–36, 2013.
- [19] ZY Jiang and ZG Qu. Lithium–ion battery thermal management using heat pipe and phase change material during discharge–charge cycle: A comprehensive numerical study. *Applied Energy*, 242:378–392, 2019.
- [20] Paolo Di Giorgio, Giovanni Di Ilio, Elio Jannelli, and Fiorentino Valerio Conte. Innovative battery thermal management system based on hydrogen storage in metal hydrides for fuel cell hybrid electric vehicles. *Applied Energy*, 315:118935, 2022.
- [21] Ziye Ling, Fangxian Wang, Xiaoming Fang, Xuenong Gao, and Zhengguo Zhang. A hybrid thermal management system for lithium ion batteries combining phase change materials with forced-air cooling. *Applied energy*, 148:403–409, 2015.
- [22] Tao Wang, KJ Tseng, Jiyun Zhao, and Zhongbao Wei. Thermal investigation of lithium-ion battery module with different cell arrangement structures and forced air-cooling strategies. *Applied energy*, 134:229–238, 2014.
- [23] Roseworthy solar farm and energy storage, June 2021.

- [24] Nam-Kyu Kim, Myung-Hyun Shim, and Dongjun Won. Building energy management strategy using an hvac system and energy storage system. *Energies*, 11(10):2690, 2018.
- [25] Petri Hietaharju, Mika Ruusunen, and Kauko Leiviskä. A dynamic model for indoor temperature prediction in buildings. *Energies*, 11(6):1477, 2018.
- [26] Tao Wang, Jiahui Fu, Menglian Zheng, and Zitao Yu. Dynamic control strategy for the electrolyte flow rate of vanadium redox flow batteries. *Applied Energy*, 227:613–623, 2018.